Available online at www.sciencedirect.com
ScienceDirect
Journal of Hazardous Materials 158 (2008) 1–13
Journal of Hazardous Materials
www.elsevier.com/locate/jhazmat

Review

Kinetic studies of elemental mercury adsorption in activated carbon fixed bed reactor

G. Skodras [a,b,c], Ir. Diamantopoulou [a,*], G. Pantoleontos [c], G.P. Sakellaropoulos [a,b]

[a] *Chemical Process Engineering Laboratory, Department of Chemical Engineering, Aristotle University of Thessaloniki, Thessaloniki, Greece*
[b] *Laboratory of Energy and Environmental Processes, Chemical Process Engineering Research Institute, Thessaloniki, Greece*
[c] *Institute for Solid Fuels Technology and Applications, Ptolemais, Greece*

Received 8 October 2007; received in revised form 21 December 2007; accepted 18 January 2008
Available online 2 February 2008

Abstract

Activated carbons are suitable materials for Hg^0 adsorption in fixed bed operation or in injection process. The fixed bed tests provide good indication of activated carbons effectiveness and service lives, which depend on the rates of Hg^0 adsorption. In order to correlate fixed bed properties and operation conditions, with their adsorptive capacity and saturation time, Hg^0 adsorption tests were realized in a bench-scale unit, consisted of F400 activated carbon fixed bed reactor. Hg^0 adsorption tests were conducted at 50 °C, under 0.1 and 0.35 ng/cm^3 Hg^0 initial concentrations and with carbon particle sizes ranging between 75–106 and 150–250 μm.

Based on the experimental breakthrough data, kinetic studies were performed to investigate the mechanism of adsorption and the rate controlling steps. Kinetic models evaluated include the Fick's intraparticle diffusion equation, the pseudo-first order model, the pseudo-second order model and Elovich kinetic equation.

The obtained experimental results revealed that the increase in particle size resulted in significant decrease of breakthrough time and mercury adsorptive capacity, due to the enhanced internal diffusion limitations and smaller external mass transfer coefficients. Additionally, higher initial mercury concentrations resulted in increased breakthrough time and mercury uptake.

From the kinetic studies results it was observed that all the examined models describes efficiently Hg^0 breakthrough curves, from breakpoint up to equilibrium time. The most accurate prediction of the experimental data was achieved by second order model, indicating that the chemisorption rate seems to be the controlling step in the procedure. However, the successful attempt to describe mercury uptake with Fick's diffusion model and the first order kinetic model, reveals that the adsorption mechanism studied was complex and followed both surface adsorption and particle diffusion.

Keywords: Adsorption kinetics; Intraparticle diffusion; Langmuir expression; Elovich model

Contents

1. Introduction . . . 2
2. Experimental . . . 4
   2.1. Samples selection and characterization . . . 4
   2.2. Mercury adsorption tests . . . 4
   2.3. Results . . . 5

* Corresponding author at: Chemical Process Engineering Laboratory, Department of Chemical Engineering, Aristotle University of Thessaloniki, P.O. Box 1520, Thessaloniki 54006, Greece. Tel.: +30 2310 994374; fax: +30 2310 996168.
E-mail address: ediamant@vergina.eng.auth.gr (Ir. Diamantopoulou).

0304-3894/$ – see front matter © 2008 Elsevier B.V. All rights reserved.
doi:10.1016/j.jhazmat.2008.01.073

2.3.1. Pore structure characterization 5
2.3.2. Mercury adsorption results 5
3. Adsorption kinetics 7
3.1. Fickian diffusion model 7
3.1.1. Theory 7
3.1.2. Results and discussion 7
3.2. Linear driving force approximation 8
3.2.1. Theory 8
3.2.2. Results and discussion 9
3.3. Pseudo-second order kinetic model 9
3.3.1. Theory 9
3.3.2. Results and discussion 10
3.4. Elovich equation 11
3.4.1. Theory 11
3.4.2. Results and discussion 11
4. Conclusions 12
References 12

1. Introduction

Mercury is a trace element of particular concern since, during coal combustion and municipal waste incineration, most of the mercury present in fuel is transferred into vapor phase, due to its high volatility. It is liberated from fuel in elemental state, $Hg^0_{(g)}$, which is the most abundant and persistent form in the atmosphere. In the post combustion environment of a boiler, it is transformed to oxidized forms ($Hg^{2+}X_{(g)}$) and particle-bound atoms ($Hg_{(p)}$). Most of the existing air pollution control technologies, such as electrostatic precipitators and baghouses, cannot remove effectively the gas phase mercury emissions, except for the particle-bound mercury atoms. Additionally, relative to the elemental mercury, the oxidized form is more effectively captured in wet scrubbers, since the $Hg^{2+}X_{(g)}$ species are generally water soluble [1].

Adsorption in solid materials is a process that offers great potential for achieving high quality air emissions with respect to mercury. However, the adsorbent must have the ability to capture all forms of gas phase mercury and convert them to a stable form that cannot be removed by wet ash-handling procedures [2]. Activated carbon is an effective adsorbent and currently has two separate applications: powdered activated carbon is injected in the flue gas stream for mercury removal and fixed bed granular activated carbon technique applied as the last treatment process, before the flue gas exits the smokestack. Although activated carbon injection upstream of a particulate control device offers a high mercury capture efficiency (>90% removal), the accomplishment of an effective mercury control with this technique, presents some disadvantages: the small contact time between the injected activated carbon and the reactant gas demands an adequate mixing of small particles with the flue gas, a high carbon to mercury ratio (C/Hg) in the flue gas resulting in a large operating cost and a sufficient mass transfer from the bulk phase to particle surface, within the small residence time in the duct [3]. On the contrary, activated carbon used in fixed bed configuration offers a larger gas/adsorbent contact time, thus requiring smaller amount of adsorbent to achieve a specific level of mercury removal [4].

In many studies, the service time and the adsorptive capacity of activated carbon column, are correlated with the adsorbent characteristics and the process parameters, such as the particle size and mercury initial concentration. Yan et al., have presented a parametric study conducted with a bench-scale fixed bed activated carbon column for mercury adsorption from flue gases. It was found that the efficiency of mercury removal was inversely proportional to the carbon size except for very fine particles that could cause high pressure drop in the column and undesirable fluidization [5]. To the same results concluded many other researchers, which have confirmed the delay of breakthrough and the reduction in mercury adsorptive capacity caused by smaller particles [6,7].

Apart from the particle size effect on mercury removal, the initial mercury concentration in flue gases entering the fixed bed reactor, has a significant impact on the adsorption behavior of activated carbons. This is of importance in field applications, where the column properties may need to be varied for flue gases with different levels of mercury. Krishnan et al., observed that the increase of initial mercury concentration promotes the mercury removal from gas phase, so long as the active sites on carbon surface are available and activated, and the mercury concentration is kept to low levels [8]. This can be attributed to the enhanced driving force for mercury mass transport, since mercury atoms have more chances to hit on carbon surface and be attached. Thus, at higher mercury concentrations, faster capturing rates and better adsorption behavior are observed [9].

The efficiencies and service lives of activated carbons need to be known for application, design and maintenance decisions, concerning the fixed bed column. These performance characteristics depend on the capacities of the carbon for the gas pollutants and the rates of adsorption of these pollutants on activated carbons surface. The rate of adsorption on activated carbon is described by the kinetics of adsorption and controls the time required to attain equilibrium [10]. A number of models are available for the kinetics of adsorption process. Some of them are derived from mass balance equations concerning

Nomenclature

a	initial adsorption rate in Elovich equation (ng/mg min)
b	desorption constant in Elovich equation (mg/ng)
c	adsorbate concentration in gas phase (ng/cm^3)
c^*	adsorbate concentration at particle surface (ng/cm^3)
C_0	reactant concentration at the surface of particle (mol/cm^3 s)
C_e	reactant gas phase concentration at equilibrium (ng/cm^3)
C_{in}	initial Hg^0 in gas phase (ng/cm^3)
C_{out}	outlet Hg^0 concentration (ng/cm^3)
d_p	particle diameter (cm)
D_{eff}	effective diffusivity (cm^2/s)
D_K	Knudsen diffusivity (cm^2/s)
D_m	molecular diffusivity (cm^2/s)
D_p	pore diffusivity (cm^2/s)
D_s	surface diffusivity (cm^2/s)
F	gas volumetric flow (cm^3/min)
h	Thiele modulus
k_a	Langmuir adsorption constant (cm^3/min ng)
k_d	Langmuir desorption constant (min^{-1})
k_f	external mass transfer coefficient (cm/s)
k_{1ads}	adsorption rate constant for first order reaction (cm/s)
k_{2ads}	adsorption rate constant for second order reaction (cm/s)
k_1	rate constant of first order equation (min^{-1})
k_2	rate constant of second order equation (mg/ng min)
K'	Henry constant
m	activated carbon mass (mg)
M	number of model parameters
M_{Hg}	mercury molecular weight
OF	objective function
q	adsorbed phase concentration averaged over a particle (ng/cm^3)
q_e	Hg^0 uptake at equilibrium (ng/mg)
q_t	Hg^0 uptake at time t (ng/mg)
r_p	pore radius (cm)
Re	Reynolds number
R_p	particle radius (cm)
Sc	Schmidt number
Sh	Sherwood number
t	adsorption time (min)
T	temperature (K)
u	fluid velocity (cm/s)
Z	number of measured data points

Greek letters

α	external surface area per unit particle volume (cm^{-1})
α'	constant into the adsorption equilibrium constant
ε	adsorbent bed voidage
ε'	effectiveness factor
ε_p	particle voidage
θ	surface coverage
μ_f	fluid viscocity (mg/s cm)
ρ_f	fluid density (mg/cm^3)
ρ_p	particle density (mg/cm^3)
τ	tortuosity factor

the external and internal diffusion process. These are the Fick's intraparticle diffusion equation and the linear driving force (LDF) kinetic model. Some others are based on pseudo-second order and Elovich kinetic equation, obtained from Langmuir and Temkin adsorption isotherms, respectively [11,12]. In most of the kinetic studies reported in the literature, heavy metals adsorption (Cr(VI), Pb(II), Cd(II), As(V), Hg(II)) from liquid phase, by means of batch experiments, has been modeled using first and second order kinetic models and Elovich kinetic equations [13,14]. They have pointed out that the majority of adsorption studies can be represented as a pseudo-first order rate mechanism. However, the pseudo-second order equation, which agrees with chemisorption as the rate controlling mechanism, is able to better describe most of the adsorption processes [15]. Regardless of the above kinetic models ability to describe mercury ions adsorption from liquid phase, there is a limited amount of information available in the literature relating to the adsorption kinetics of gas phase elemental mercury on activated carbons. Some studies have been associated with the adsorption of organic vapors (methanol, ethanol), water molecules, carbon dioxide, nitrogen and oxygen, on carbon molecular sieves and activated carbons. The two simplest approaches that are used are the Fick's diffusion law for homogenous materials or some other models, including the linear driving force mass transfer model and the Langmuir second order model. The target of this analysis is to determine the existence of a particular mechanism for the adsorption process and to elucidate whether the diffusion inside the particle follows the Fickian model. Among the examined models, in most of the cases the second order equation can accurately describe the rate of uptake of gases [16,17].

The objective of this work is to assess the potential of the commercial activated carbon F400 used in a fixed bed operation for the adsorption of elemental mercury from N_2 flow. Four simplified kinetic models, including intraparticle diffusion model, pseudo-first- and pseudo-second order equations, and Elovich model, were used to describe the adsorption process and to investigate the mechanism of mercury adsorption and the potential rate controlling steps, such as mass transport and chemisorption. The rates and the adsorptive capacity of the examined activated carbon, as well as the validity of each kinetic model, were examined by varying the initial mercury concentration and the particle size of activated carbon. The small particle size and the high initial mercury concentration enhanced mercury removal and attained increased equilibrium times. Although these experimental data were predicted successfully by the kinetic models

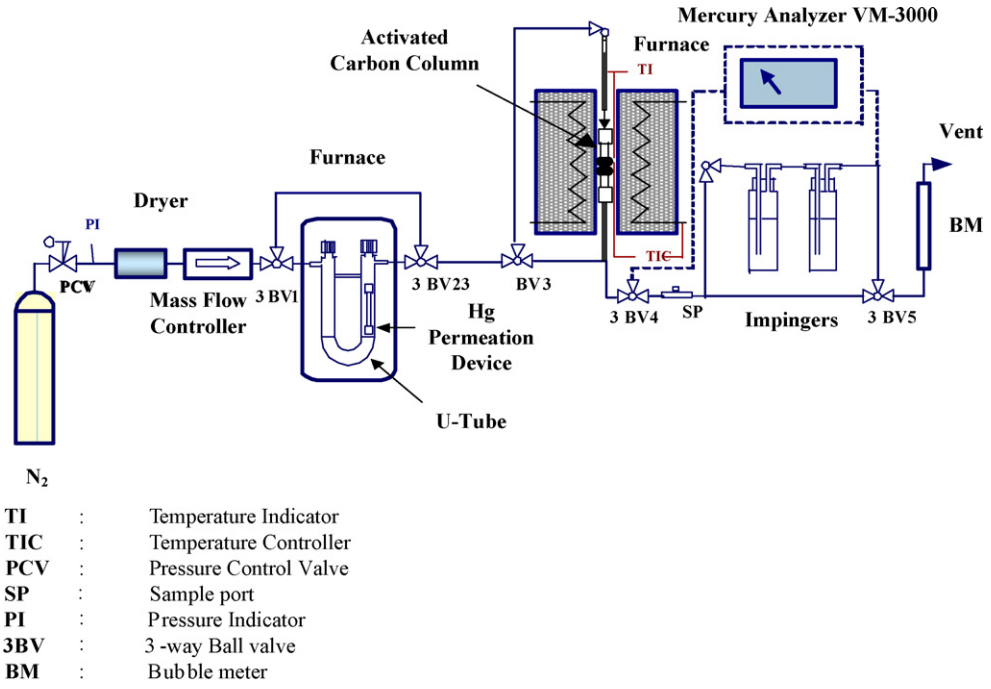

Fig. 1. Hg^0 adsorption unit.

tested, the best fitting results were obtained by a pseudo-second order kinetic model. This indicates that the adsorption process is controlled by the chemisorption mechanism. However, the accurate prediction of experimental results with the internal diffusion model and the first order equation, prove that the mass transfer limitations cannot be ignored.

2. Experimental

2.1. Samples selection and characterization

Mercury adsorption experiments were performed using the commercial activated carbon, Calgon F400. Physical adsorption methods (N_2 adsorption at 77 K and CO_2 adsorption at 298 K) were employed to characterize its pore structure. A conventional volumetric apparatus (Quantasorb Co.) was used for the N_2 and CO_2 adsorption experiments. The adsorbed volumes of N_2 and CO_2 are expressed as Scm^3 (referred to Standard conditions). BET and Dubinin-Raduchevich equations were used to calculate surface areas, total pore volumes and micropore volumes from N_2 ($V_{\mu_p}^{N_2}$) and CO_2 adsorption ($V_{\mu_p}^{CO_2}$).

2.2. Mercury adsorption tests

A schematic representation of mercury adsorption unit is shown in Fig. 1. Mercury adsorption tests were conducted with 20 mg activated carbon mass, mixed with 1 g of sand, in a differential-fixed bed reactor (0.635 cm inner diameter stainless steel column), enclosed in a temperature-controlled oven. The adsorption unit is described with more details elsewhere [18]. To account for the effects of particle size on mercury adsorption, tests were performed on F400 activated carbon particles, ranging in 75–106 and 150–250 μm, while the adsorption temperature was 50 °C. A mercury permeation device was used as a source of elemental mercury Hg^0 (VICI Metronics Inc., Santa Clara, CA). The device, designed to produce constant release of mercury vapor per unit time at the specified temperatures, was secured in a temperature-controlled stainless steel U-tube holder,

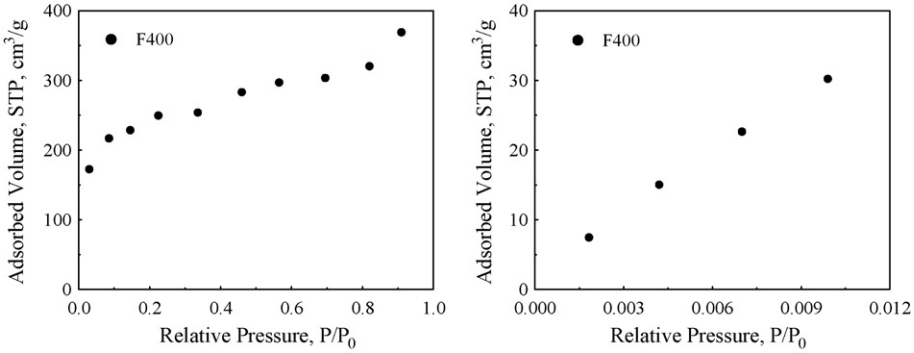

Fig. 2. N_2 and CO_2 adsorption isotherms of F400 activated carbon.

Table 1
Pore structure characteristics of F400 activated carbon

Sample	Specific surface area BET (m^2/g)	CO_2 area (m^2/g)	Total pore volume V_{tot} (cm^3/g)	N_2 micropore volume $V_{\mu_p}^{N_2}$ (cm^3/g)	% Micropores contribution $V_{\mu_p}^{N_2}$ % V_{tot}	CO_2 micropore volume $V_{\mu_p}^{CO_2}$ (cm^3/g)
F400	827.3	840.1	0.52	0.4	77	0.23

while nitrogen at preadjusted constant flow was fed through it. A mass flow controller kept the nitrogen flow constant, at 200 cm^3/min. By varying the temperature of mercury permeation device, the mercury inlet concentration was adjusted at 0.1 and 0.35 ng/cm^3. For the continuous measurement of the gas phase elemental mercury concentration, a Mercury Instruments Analyzer (Combination model VM-3000-LabAnalyzer 254) was used, based on cold vapor absorption spectrometry.

In order to equilibrate the carrier gas flow rate in the system, two three way valves, placed immediately upstream and downstream of the U-tube holder, were used to bypass the permeation device when flushing the system with clean carrier gas. The clean nitrogen was directed through the empty reactor. Then the mercury permeation device was placed on line while the temperature of the oven was adjusted to generate the desired mercury concentration. At the same time, the bypassed reactor was charged with the adsorbent and heated at the desired adsorption temperature. When the later was achieved, the mercury gas stream was passed through the fixed bed reactor initializing the adsorption time.

In order to calculate activated carbon adsorptive capacity, mercury breakthrough curves through the fixed bed column, have been constructed, by employing mercury measured concentrations in gas phase. The repeatability of the experimental breakthrough curves was tested by employing the

2.3. Results

2.3.1. Pore structure characterization

The N_2 and CO_2 adsorption isotherms of F400 activated carbon, are illustrated in Fig. 2, and they were used for calculating the BET and CO_2 surface areas, total pore volume and micropore volume contribution, Table 1. The pore structure characteristics obtained from N_2 and CO_2 adsorption isotherms of F400 indicate a well developed pore and micropore structure, Fig. 2. This is further evident by the high BET and CO_2 surface area, the total and the micropore volume of the sample given in Table 1.

2.3.2. Mercury adsorption results

2.3.2.1. Particle size effect. Mercury breakthrough curves for F400 activated carbon with particle size of 75–106 and 150–250 μm are given in Fig. 3a. The initial mercury concentration was 0.35 ng/cm^3 and the adsorption temperature was adjusted at 50 °C. Breakthrough curves derived from adsorption on F400 activated carbon, with particle size ranging between 150–250 μm, and initial mercury concentration of 0.1 ng/cm^3, are exposed in Fig. 3b. F400 adsorptive capacities calculated by integrating these breakthrough curves, during 360 min adsorption experiment, are presented in Table 2.

As it is observed, the increase in particle size from 75–106 to 150–250 μm resulted in a significant decrease in the breakthrough time and mercury adsorptive capacity, Fig. 3a, Table 2. It seems that smaller particle produces a delay of the breakthrough, while the larger one can cause the opposite effect. That is, in the finer particle size ranges, adsorption breakthrough curves follow a much more efficient profile than that in larger particle size ranges, since the breakthrough time increases and the breakthrough curve tends towards the classic "S" shaped profile [19]. Thus, for small particle sizes, F400 adsorptive capacity is higher than the mercury adsorbed quantity that is disposed by other commercial products (Norit FGD, 450–618 ng/mg), [20]. This observation can be quantified using the well-known relation between the Thiele modulus h and spherical particle radius R_p, expressed for first and second order kinetics, [21] as:

$$h_1 = R_p \sqrt{k_1 S_g \frac{\rho_p}{D_{eff}}} \quad (1)$$

$$h_2 = R_p \sqrt{k_{2(ads)} S_g \rho_p \frac{C_0}{D_{eff}}} \quad (2)$$

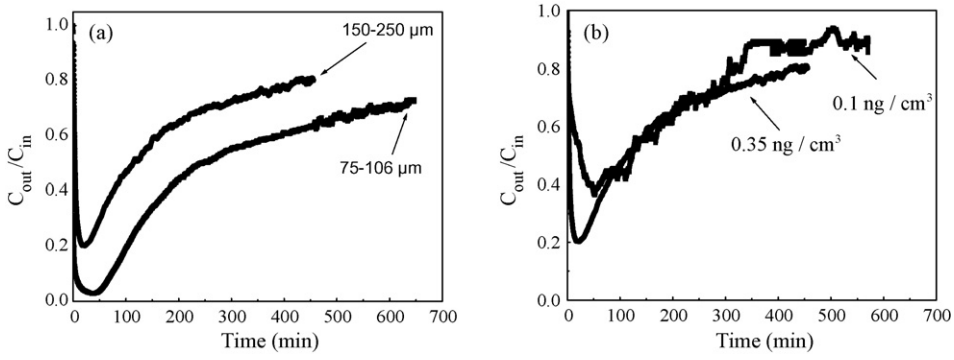

Fig. 3. Hg^0 breakthrough curves from F400 activated carbon. Adsorption temperature: 50 °C. (a) Particle size effect. (b) Initial concentration effect.

Table 2
Effect of particle size on mercury adsorption

Particle diameter d_p (μm)	Mean radius R_p (cm)	Breakpoint t_b (min)	Hg^0 adsorptive capacity at breakpoint (ng/mg)	Total breakthrough time (min)	Hg^0 adsorptive capacity q (ng/mg)*
75–106	0.0045	39	154	530	707
150–250	0.01	22	47	397	505

* signifies 360 min adsorption experiment, 50 °C adsorption temperature.

where R_p (cm) is the particle radius, $k_{1(ads)}$ and $k_{2(ads)}$ (cm/s) are the adsorption rate constants, ρ_p (mg/cm^3) is the particle density, S_g (cm^2/mg) is the surface area per mg of adsorbent, D_{eff} (cm^2/s) is the effective diffusivity and C_0 (mol/cm^3 s) is the reactant concentration at the surface of the particle.

The Thiele modulus expressions, Eqs. (1) and (2), that are defined as the ratio of an intrinsic reaction rate in the absence of mass transfer limitations to the rate of diffusion into the particles under specified conditions, imply that the observed rate of adsorption is inversely proportional to the particle size. This means that when the particle size increases, Thiele modulus becomes larger and the adsorption is diffusion limited within the spherical particle. Thus, the ability of the system to diffuse the reactants insight the pores is limited, while the adsorption is fast. Consequently, the reactant is consumed at the outer surface of the particle, the breakthrough curves become steeper and faster, and the breakthrough time decreases. In this case, the effectiveness factor ε' that is expressed by Eq. (3), is reduced to:

$$\varepsilon' = \frac{1}{h}\left[\frac{1}{\tan 3h} - \frac{1}{3h}\right] \tag{3}$$

Apart from the effect on internal diffusion limitations, the particle size of activated carbon influences the external mass transfer coefficient k_f, that is calculated by the following equation:

$$k_f = \frac{Sh D_m}{2R_p} \tag{4}$$

where D_m (cm^2/s) is the molecular diffusivity, k_f (cm/s) is the external mass transfer coefficient, Sh is the Sherwood number and R_p (cm) is the particle radius.

The Sherwood number is defined as:

$$Sh = \frac{1.09}{\varepsilon} Re^{0.33} Sc^{0.33} \tag{5}$$

where Re is the Reynolds number in the fixed bed, Sc is the Schmidt number and ε is the void volume of the adsorbent bed.

Reynolds and Schmidt numbers are estimated by the following equations:

$$Re = \frac{(2R_p)u\rho_f}{\mu_f(1-\varepsilon)} \tag{6}$$

$$Sc = \frac{\mu_f}{\rho_f D_m} \tag{7}$$

where u (cm/s) is the fluid velocity, ρ_f (mg/cm^3) is the fluid density and μ_f (mg/s cm) is the fluid viscosity.

The effective diffusivity is defined as:

$$D_{eff} = \frac{\varepsilon_p}{\tau} \frac{1}{((1/D_K) + (1/D_m))} \tag{8}$$

where ε_p is the particle void volume, τ is the tortuosity factor and D_K (cm^2/s) is the Knudsen diffusivity.

The Knudsen diffusivity may be estimated from the expression:

$$D_K = 9700 r_p \left(\frac{T}{M_{Hg}}\right)^{1/2} \tag{9}$$

where D_K (cm^2/s) is the Knudsen diffusivity, r_p (cm) is the pore radius, T (K) is the temperature and M_{Hg} is mercury molecular weight.

When the particle size increases, the external mass transfer coefficient and the external surface area per unit particle volume decrease, while pore diffusivity remains the same, Table 3. This causes the decrease of the mass transfer rate through the external particle layer and of the adsorption rate of mercury on activated carbon particle, Eq. (10), [22]:

$$\frac{\partial q}{\partial t} = k_f a(c - c^*) = \frac{3k_f}{R_p}(c - c^*) \tag{10}$$

where q (ng/cm^3) is the adsorbed phase concentration averaged over a particle, α (cm^{-1}) is the external surface area per unit particle volume, c (ng/cm^3) is adsorbate concentration in gas phase and c^* (ng/cm^3) is the adsorbent concentration at particle surface.

2.3.2.2. Initial concentration effect. The increase of the initial concentration from 0.1 to 0.35 ng/cm^3 causes the decrease in breakpoint from 52 to 22 min, Fig. 3b and Table 4. This can be attributed to the effective pore diffusivity decrease with increasing initial mercury concentration, that is illustrated by Eq. (11),

Table 3
Physical properties of F400 particle and reactant gas

	Particle Size	
	75–106 μm	150–250 μm
R_p (cm)	0.0045	0.01
r_p (cm)	2.418 E-07	2.418 E-07
ε_p	0.5	0.5
ε	0.4	0.4
ρ_f (mg/cm^3)	1.056	1.056
μ_f (mg/s cm)	0.2	0.2
Re	0.84	1.87
D_m (cm^2/s)	0.15	0.15
D_{eff} (cm^2/s)	0.001	0.001
Sc	1.23	1.23
Sh	2.73	3.55
k_f (cm/s)	46.62	27.3

External and internal mass transfer coefficients.

Table 4
Effect of initial mercury concentration on mercury adsorption

Hg^0 initial concentration C_{in} (ng/cm^3)	Breakpoint t_b (min)	Hg^0 adsorptive capacity at breakpoint (ng/mg)	Total breakthrough time (min)	Hg^0 adsorptive capacity q (ng/mg)*
0.1	52	24	329	130
0.35	22	47	397	505

* signifies 360 min adsorption experiment, 50 °C adsorption temperature.

[16].

$$D_{eff} = D_p + \frac{1-\varepsilon_p}{\varepsilon_p}\frac{\partial q}{\partial c}D_s \quad (11)$$

where D_p (cm^2/s) is the pore diffusivity, D_s (cm^2/s) is the surface diffusivity.

However, the total breakthrough time of mercury through fixed bed column increased from 329 to 397 min and F400 mercury adsorptive capacity calculated at 360 min adsorption experiment improved from 130 to 505 ng/mg, Table 4. It can be observed that the mercury adsorptive capacity increases almost linearly with an increase in influent mercury concentration, which suggests that under the experimental conditions used, mercury adsorption on F400 activated carbon occurs in Henry's law region, and the higher mercury concentration provides a higher driving force to facilitate mercury uptake [23]. According to Henry's law, Eq. (12), for physical adsorption on a uniform surface at sufficiently low concentrations, the equilibrium relationship between gas phase and adsorbed phase concentrations will be linear [22].

$$q = K'c \quad (12)$$

where K' is the Henry constant.

3. Adsorption kinetics

In order to investigate the mechanism of gas phase mercury adsorption on activated carbons, and the potential rate controlling steps, such as mass transport and chemical reaction process, kinetic models have been used by employing the data derived from Hg^0 adsorption experiments. Based on the assumption that the adsorption of mercury on activated carbons involves many processes, such as external mass transfer between the external surfaces of the adsorbent particles and the surrounding fluid phase, intraparticle transport mechanisms (pore diffusion, surface diffusion in the adsorbed phase) and adsorption, two approaches can be used: the application of Fick's diffusion law or the description of the process by models based on Langmuir adsorption rate expression and Temkin isotherm. The effects of initial mercury concentration and activated carbon particle size were analyzed from the kinetic point of view, due to their influence on mercury adsorption rate.

The theoretical analysis is limited to an isothermal, of constant pressure system, involving adsorption of a single adsorbate component on a spherical particle of adsorbent. Axial dispersion is neglected and the gas velocity is assumed to be uniform throughout the column.

3.1. Fickian diffusion model

3.1.1. Theory

When internal diffusion steps control the process, one of the simplest approaches for an approximate description of adsorption, in terms of rate coefficients, is the Fick's diffusion model. In this case, the diffusion behavior inside a spherical homogenous particle can be derived from Fick's law, which can be used to describe both pore and solid diffusion. In the diffusion model, the diffusivity is independent of the vacant site concentration on the surface and will be constant only for thermodynamically ideal systems [24].

The kinetic expression derived from Fick's diffusion model, is given by the following equation [22]:

$$\frac{q_t}{q_e} = 1 - \frac{6}{\pi^2}\sum_{n=1}^{\infty}\frac{1}{n^2}\exp\left(-\frac{n^2\pi^2 D_{eff}t}{R_p^2}\right) \quad (13)$$

where q_t (ng/mg) is the Hg^0 uptake at time t and q_e (ng/mg) is the Hg^0 uptake at equilibrium.

The computational approach used actually forces experimental data to fit to a proposed model, by finding the unknown parameters in a manner that minimizes deviation between experimental and calculated data. In this work, the latter is achieved using the unweighted least squares estimation, that is, the minimization of the sum of squares of errors without any weighting factor [25]. Particularly, the parameters of interest, $\pi^2 D_{eff}/R_p^2$ and q_e, were evaluated by minimizing the square of the difference of the experimental vector minus the theoretical one, derived by the diffusion equation (Eq. (13)). The optimisation procedure comprises a non-linear model fitting problem, which was solved using Maple 10/Global Optimization Toolbox (GOT). For various n, the latter combines the flexibility of using analytical expressions, such as Eq. (13) with techniques for finding global minima over a wide range.

3.1.2. Results and discussion

In order to apply the Fickian diffusion model and examine its ability to describe the rate of mercury uptake from gas phase, the amount of Hg^0 adsorbed at time t, based on Hg^0 breakthrough curves presented in Fig. 3, was calculated from the mass balance equation:

$$q_t = \frac{F}{m}(C_{in} - C_{out})t \quad (14)$$

where q_t (ng/mg) is the Hg^0 uptake at time t, C_{in} (ng/cm^3) is the initial Hg^0 concentration in gas phase, C_{out} (ng/cm^3) is the outlet Hg^0 concentration, F (cm^3/min) is the volumetric flow of

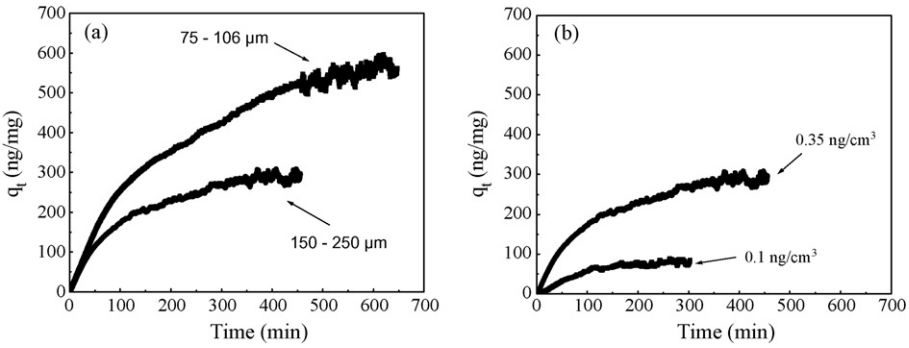

Fig. 4. Variation of Hg^0 uptake with time. Adsorption on F400 activated carbon at 50 °C. (a) Particle size effect. (b) Initial concentration effect.

gas mixture, m (mg) is the activated carbon mass and t (min) is the time of adsorption.

The experimental Hg^0 uptake curves are presented in Fig. 4. The estimation of the best fitting parameters q_e and $\pi^2 D_{eff}/R_p^2$, is achieved through the deviation between experimental and calculated curves of Hg^0 uptake at time t, as a percentage of the maximum experimental value (q), [26]:

$$\mathrm{DEV}(\%) = \frac{\sqrt{\mathrm{OF}/(Z-M)}}{\max(q_{t\,\mathrm{pred}})} \quad (15)$$

where DEV(%) is the percentage of deviation, OF is the objective function, Z is the number of measured data points, M is the number of model parameters and q_{exp} (ng/mg) is the experimental Hg^0 uptake, $\max(q_{t\,\mathrm{pred}})$ (ng/mg) is the maximum predicted Hg^0 uptake.

The use of objective function involves the minimization of the differences of squares between the experimental and predicted data:

$$\mathrm{OF} = \sum_{1}^{n} (q_{t\,\mathrm{exp}} - q_{t\,\mathrm{pred}})^2 \quad (16)$$

where $q_{t\,\mathrm{exp}}$ (ng/mg) is the experimental Hg^0 uptake and $q_{t\,\mathrm{pred}}$ (ng/mg) is the predicted Hg^0 uptake.

The theoretical curves obtained for different activated carbon particle size and initial mercury concentrations, and compared to experimental curves, are illustrated in Fig. 5a. Based on these results, the theoretical breakthrough curves have been produced by employing Eq. (14), Fig. 5b. The calculated parameters q_e and $\pi^2 D_{eff}/R_p^2$, and the percentage of deviation between experimental and theoretical uptake curves, are presented in Table 5. The results presented in Fig. 5a, as well as in Table 5, indicate that the Fick's diffusion model approaches efficiently the rate of Hg^0 adsorption, since the percentage of deviation is less than 5%, in most of the cases. This model can also describe Hg^0 breakthrough curves, from the breakpoint up to equilibrium time, Fig. 5b. However, for low initial mercury concentration, (0.1 ng/cm^3), the diffusion model prediction deviates considerably from experimentally obtained data, Table 5. This observation is in agreement with the theory that predicts that external film diffusion controls the process when the adsorbate concentration is very low. Finally, the kinetic constant calculated by diffusion model increased with the adsorbent particle size, resulting in fast fixed bed saturation and small breakthrough times demand. This confirms the conclusion derived from experimental results, which demonstrate the increase of the gas film resistance and of the interior diffusion path with the increase of particle size.

3.2. Linear driving force approximation

3.2.1. Theory

The Hg^0 gas uptake into activated carbons may be considered as a pseudo-first order mass transfer mechanism between the gas phase and the carbon adsorption sites. The linear driving force approximation is obtained when the driving force is expressed as a concentration difference. It was originally devel-

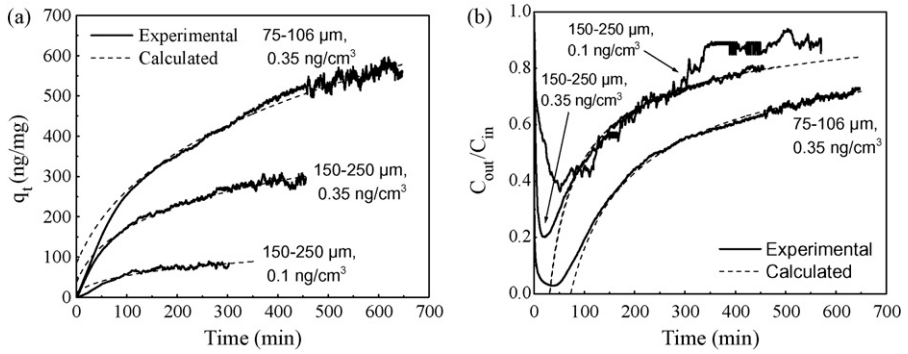

Fig. 5. Kinetic analysis of Hg^0 adsorption on F400 activated carbon at 50 °C, by intraparticle diffusion model. (a) Variation of Hg^0 uptake with time. (b) Experimental and calculated Hg^0 breakthrough curves.

Table 5
Kinetic data obtained by diffusion model for Hg^0 adsorption on F400 activated carbon

Initial concentration $C_{Hg\ (in)}$ (ng/cm^3)	Particle size d_p (μm)	Experimental Hg^0 adsorption capacity $q_{e\ (exp)}$ (ng/mg)	Calculated Hg^0 adsorption capacity $q_{e\ (pred)}$ (ng/mg)	Deviation % (DEV %)	Kinetic constant $K_{diffus.}$ ($\pi^2\ D_{eff}/R_p^2$) (min^{-1})
0.35	150–250	505	386	3.84	0.00285
	75–106	1003	906	3.84	0.000872
0.1	150–250	130	131	8.17	0.00192

Adsorption temperature: 50 °C.

oped to describe packed-bed dynamics under linear equilibrium conditions and is generally expressed as follows [27]:

$$\frac{dq_t}{dt} = k_1(q_e - q_t) \Rightarrow q_t = q_e[1 - \exp(-k_1 t)] \quad (17)$$

where q_t and q_e are Hg^0 uptake at time t and at equilibrium, respectively (ng/mg) and k_1 is the rate constant of pseudo-first order equation (min^{-1}).

This form is exact for a non-linear isotherm only when external mass transfer is controlling the process. However, it can also be used for non-linear systems with pore or surface diffusion mechanisms, as an approximation [28]. The main advantage of this approximation is in its simplified formulas for unsteady state diffusion in porous particles. Thus, it has been developed only for no-reaction cases and cannot distinguish between the adsorbed and the diffusing phase, which are normally distinguishable in the case of adsorption in porous particles. However, there are many researchers who have employed the pseudo-first order kinetic equation in order to describe reaction, adsorption and unsteady state diffusion phenomena [29].

3.2.2. Results and discussion

The kinetic data of Fig. 4 analyzed using the LDF model, are presented in Eq. (17). Experimental data are forced to fit this equation by estimating the observed rate constant, k_1, and the adsorption capacity at equilibrium, q_e, using the non-linear regression methods. The fitted curves of the pseudo-first order kinetic model along with the experimental data, are illustrated in Fig. 6a, for comparison. Based on these results, the theoretical breakthrough curves have been produced by employing Eq. (14), Fig. 6b. The calculated parameters k_1 and q_e, as well as the percentage of deviation between experimental and theoretical uptake curves, are presented in Table 6.

The calculated uptake curves presented in Fig. 6a, approach the experimental ones, while the % deviations obtained, were lower compared to the deviations derived from the intraparticle diffusion model, Tables 5 and 6. Thus, the linear driving force model seems to describe the experimental kinetic data more closely, compared to the internal diffusion model, indicating that the surface diffusion mechanism probably controls the mass transport process in activated carbon particle. On the contrary, the resistance in molecular diffusion through the external film around the particle, seems to be negligible, since the external film diffusion coefficient (k_f) is higher than effective diffusion coefficient (D_{eff}), Table 3. However, the theoretical equilibrium adsorption capacity, q_e, is smaller than the one obtained from diffusion model, deviating from the experimental values, Table 6. It is also obvious that by increasing the initial mercury concentration from 0.1 to 0.35 ng/cm^3, the deviation between the experimental and calculated data decreases. This conclusion is in agreement with the results presented in many studies, which indicate that the adsorption process obeys pseudo-first order kinetics when the initial concentration of reactant is too high [30].

3.3. Pseudo-second order kinetic model

3.3.1. Theory

While the LDF model is used for both extraparticle and intraparticle mass transfer mechanisms, the reaction kinetics approximation is usually employed for systems where the reaction step at pore surfaces is the controlling step. In these cases, the mass transfer parameter that is determined by diffusion and

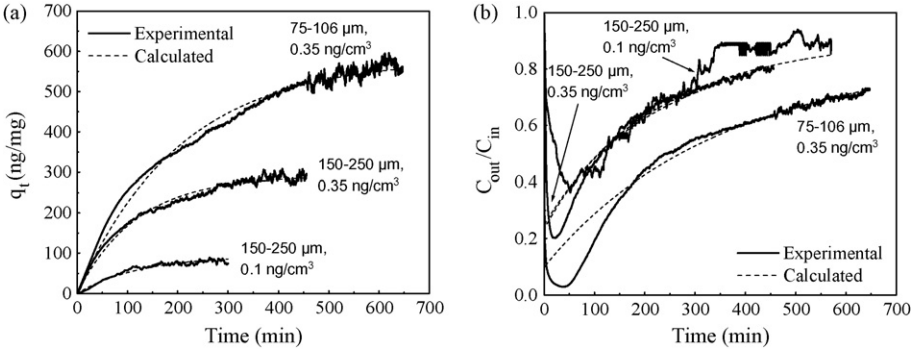

Fig. 6. Kinetic analysis of Hg^0 adsorption on F400 activated carbon at 50 °C, by pseudo-first order kinetic model. (a) Variation of Hg^0 uptake with time. (b) Experimental and calculated Hg^0 breakthrough curves.

Table 6
Kinetic data obtained by pseudo-first order kinetic model for Hg^0 adsorption on F400 activated carbon

Initial concentration $C_{Hg\ (in)}$ (ng/cm^3)	Particle size d_p (μm)	Experimental Hg^0 adsorption capacity $q_{e\ (exp)}$ (ng/mg)	Calculated Hg^0 adsorption capacity $q_{e\ (pred)}$ (ng/mg)	Deviation % (DEV %)	Kinetic constant k_1 (mg/ng min)
0.35	150–250	505	291.52	3.16	0.0085
	75–106	1003	581.56	3	0.0048
0.1	150–250	130.6	94.05	5.39	0.008

Adsorption temperature: 50 °C.

linear driving force kinetic models, is replaced by a second order reaction rate constant, k_2 [11]. Thus, when the process may be pseudo-second order and the rate limiting step may be chemisorption, the kinetic model based on Langmuir type second order mass action rate expression, has been used to describe the adsorption dynamics [31]. pseudo-second order kinetic model constitutes a mass action rate model where the surface diffusivity is inversely proportional to the square of concentration of vacant sites in surface [17].The rate expression for the adsorption is described by Eq. (18):

$$\frac{dq_t}{dt} = k_2(q_e - q_t)^2 \Rightarrow \frac{t}{q_t} = \frac{1}{k_2 q_e^2} + \frac{t}{q_e}$$
$$\Rightarrow q_t = \frac{t}{(1/(k_2 q_e^2)) + (t/q_e)} \quad (18)$$

where q_t and q_e are Hg^0 uptake at time t and at equilibrium, respectively (ng/mg) and k_2 is the rate constant of pseudo-second order equation (mg/ng min). The term $k_2 q_e^2$ can be regarded as the initial adsorption rate

In this case the adsorption follows the Langmuir equation, which is obtained based on the assumptions associated with an ideal uniform surface [32]:

$$\frac{d\theta}{dt} = k_a c(1-\theta) - k_d\theta \quad (19)$$

where θ is the surface coverage (q_t/q_e), k_a is the Langmuir adsorption constant (cm^3 min^{-1} ng^{-1}) and k_d is the Langmuir desorption constant (min^{-1}).

This expression of pseudo-second order rate of adsorption is based on the adsorption capacity on the solid surface and has the following advantages: the adsorption capacity, the rate constant and the initial adsorption rate can be determined from Eq. (19), [33].

3.3.2. Results and discussion

The validity of pseudo-second order kinetic model has been checked by studying the kinetics under different initial mercury concentrations and adsorbent particle sizes, Fig. 4. Experimental data are forced to fit Eq. (20) by estimating the observed rate constant, k_2, and the adsorption capacity at equilibrium, q_e, using non-linear regression methods. Fig. 7a shows the experimental mercury uptake curves in relation to the curves calculated from the constants (k_2, q_e) derived from pseudo-second order model solution, Table 7. Based on these results, the theoretical breakthrough curves have been produced by employing Eq. (14), Fig. 7b. The calculated parameters k_2 and q_e, as well as the percentage of deviation between experimental and theoretical uptake curves, are presented in Table 7.

A very good agreement between the experimental data and the modeled curves derived from pseudo-second order equation was obtained, Fig. 7a, just as in the case of pseudo-first order and internal diffusion kinetic models application. However, % deviations between experimental and theoretical adsorption curves are much lower in the case of pseudo-second order kinetic model. This suggests that the adsorption system studied belongs to the second order kinetic model that expresses the chemisorption's nature of the adsorption process [34]. The particle size increase resulted in an increase of the kinetic constant k_2, indicating that the larger particle size provides faster adsorption kinetics and smaller breakthrough times, Table 7. This observation is in agreement with the experimental results regarding the effect of particle size variation on mercury uptake, Fig. 3.

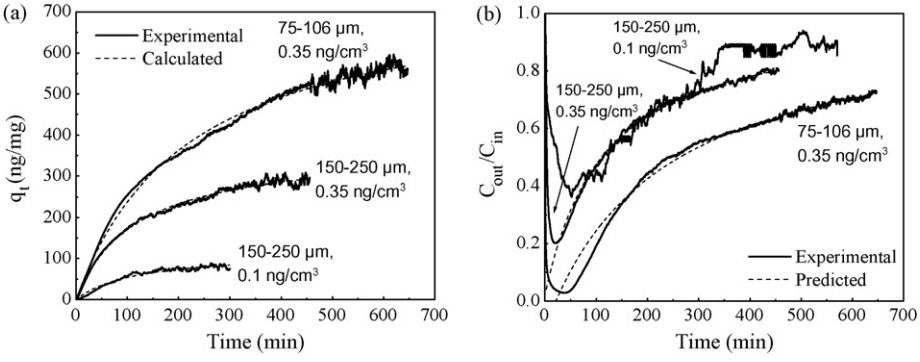

Fig. 7. Kinetic analysis of Hg^0 adsorption on F400 activated carbon at 50 °C, by pseudo-second order kinetic model. (a) Variation of Hg^0 uptake with time. (b) Experimental and calculated Hg^0 breakthrough curves.

Table 7
Kinetic data obtained by pseudo-second order kinetic model for Hg^0 adsorption on F400 activated carbon

Initial concentration $C_{Hg\ (in)}$ (ng/cm^3)	Particle size d_p (μm)	Experimental Hg^0 adsorption capacity $q_{e\ (exp)}$ (ng/mg)	Calculated Hg^0 adsorption capacity $q_{e\ (pred)}$ (ng/mg)	Deviation % (DEV %)	Kinetic constant k_2 (mg/ng min)	Initial adsorption rate $k_2\ q_e^2$ (ng/mg min)
0.35	150–250	505	368.18	2.25	2.35 E-05	3.18
	75–106	1003	763.18	1.28	5.93 E-06	3.45
0.1	150–250	130.6	117.58	5.34	7.2 E-05	1

Adsorption temperature: 50 °C.

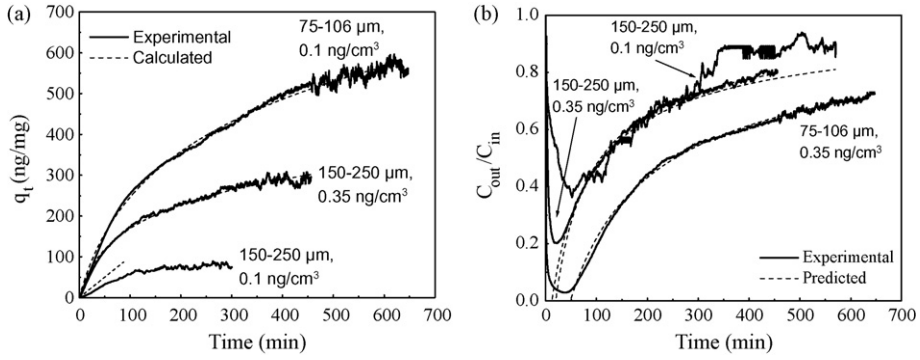

Fig. 8. Kinetic analysis of Hg^0 adsorption on F400 activated carbon at 50 °C, by Elovich kinetic model. (a) Variation of Hg^0 uptake with time. (b) Experimental and calculated Hg^0 breakthrough curves.

3.4. Elovich equation

3.4.1. Theory

Additionally to Langmuir adsorption kinetic model, Elovich equation, is another expression based on the adsorptive capacity of adsorbents and describes the kinetics of gas chemisorption on solids. If in adsorption systems equilibrium is described by Temkin empirical equation, then the adsorption kinetics is expressed well by Elovich model. This was observed commonly in adsorption systems with strong heterogeneous solid surfaces, such as the catalyst surfaces [35].

Temkin equation is represented in the following way:

$$q_e = \frac{RT}{b} \ln(aC_e) \tag{20}$$

where q_e is the Hg^0 uptake at equilibrium (ng/mg), b is the desorption constant (mg/ng), a is the constant that expresses the initial adsorption rate (ng/mg min) and C_e is the reactant gas phase concentration at equilibrium (ng/cm^3).

The Elovich equation is formulated as:

$$\frac{dq_t}{dt} = a \exp(-bq_t) \tag{21}$$

where q_t is mercury uptake at time t (ng/mg).

Integrating the rate equation using the initial condition: $q(t=0)=0$, Eq. (21) becomes:

$$q_t = \frac{2.3}{a} \log(1 + abt) \tag{22}$$

Eq. (22) will be used to test the applicability of the Elovich model to the kinetics of adsorption.

3.4.2. Results and discussion

The theoretical curves generated from the solution of the Elovich equation, Eq. (22), using non-linear regression methods, are illustrated in Fig. 8a. The results of kinetic data fitting to Elovich model are presented in Table 8, which contains the estimated parameters α and b, the % deviation between experimental and theoretical adsorption curves and the calculated adsorptive capacity at equilibrium, q_e. Based on these results, the theoret-

Table 8
Kinetic data obtained by Elovich kinetic model for Hg^0 adsorption on F400 activated carbon

Initial concentration $C_{Hg\ (in)}$ (ng/cm^3)	Particle size d_p (μm)	Experimental Hg^0 adsorption capacity $q_{e\ (exp)}$ (ng/mg)	Calculated Hg^0 adsorption capacity $q_{e\ (pred)}$ (ng/mg)	Deviation % (DEV %)	Constant a (ng/mg min)	Constant b (min^{-1})
0.35	150–250	505	299	5.58	0.01035	4.624
	75–106	1003	580	1.68	0.0046	4.586
0.1	150–250	130.6	87.18	6	0.027	0.0362

Adsorption temperature: 50 °C.

ical breakthrough curves have been derived by employing Eq. (14), Fig. 8b.

Using Elovich kinetics, Fig. 8a, show an excellent agreement between the experimental data and the theoretical adsorption curves, in the whole adsorption time, while the calculated breakthrough curves, Fig. 8b, are close to the experimental ones, from the breakpoint up to equilibrium time. Mercury adsorption with initial concentration 0.1 ng/cm^3 comprises an exception, Fig. 8b. However, q_e values calculated from Elovich kinetic model do not agree with the experimental values, while q_e values obtained from the internal diffusion, pseudo-first and pseudo-second order kinetic models are close to the experimental ones, Tables 5–8. In the same way, Elovich equation shows higher percentage of deviation between experimental data and theoretical uptake curves, compared to the pseudo-second order kinetic model, Tables 7 and 8. Hence, the adsorption system is better described by the pseudo-second order kinetic model and the Langmuir isotherm, which are based on the assumption that the rate determining step may be chemisorption [36].

4. Conclusions

The removal of gas phase elemental mercury by the commercial activated carbon F400 was studied in packed-bed experiments. The examined adsorbent disposes high BET surface area, total pore volume and micropore volume contribution, compared to various materials reported in the literature. When some of the adsorption experiments conditions and the fixed bed characteristics (Hg^0 gas phase concentration, carbon particle size) vary, F400 demonstrated Hg^0 adsorptive capacity ranging from lower to higher, compared to other commercial products. For larger feed concentration, breakthrough time was achieved later and fixed bed behavior was improved. The same conclusions have been extracted with the decrease in particle radius.

In order to formulate a general expression describing the kinetics of gas phase mercury adsorption on activated carbons, and to predict mercury adsorptive capacity and column saturation time, several kinetic equations have been examined, and their results have been compared. These are the Fick's intraparticle diffusion equation, the first- and second order model and the Elovich kinetic equation.

From the kinetic studies results, it was observed that the intraparticle diffusion model described by the Fick's law, approaches the rate of the mercury uptake, especially at higher initial concentrations, and predicts the equilibrium adsorptive capacity more accurately than the linear driving force model. The later describes the process well at increased mercury concentration, but cannot describe the experimental breakthrough data closely. Although the mass transfer limitations affect the overall mercury uptake, the chemical adsorption rate seems to be the slow and controlling step during mercury removal procedure. This is indicated by the suitability of the second order equation. Apart from the second order model, the chemisorption rate was also expressed by the Elovich kinetic equation. However, the results obtained by this equation deviate from the experimental data more than that of the theoretical results derived from the second order model. Thus, the rate of chemisorption obeys the pseudo-second order model and the equilibrium data follows the Langmuir isotherm, since the Langmuir rate expression produces this model.

References

[1] K.C. Galbreath, C.J. Zygarlicke, Mercury transformations in coal combustion flue gas, Fuel Process. Technol. 65–66 (2000) 289–310.
[2] J.D. Laumb, S.A. Benson, E.A. Olson, X-ray photoelectron spectroscopy analysis of mercury sorbents surface chemistry, Fuel Process. Technol. 85 (2004) 577–585.
[3] S.J. Miller, G.E. Dunham, E.S. Olson, T.D. Brown, Flue gas effects on a carbon-based mercury sorbent, Fuel Process. Technol. 65–66 (2000) 343–365.
[4] F. Scala, Simulation of mercury capture by activated carbon injection in incinerator flue gas. 2. Fabric filter removal, Environ. Sci. Technol. 35 (2001) 4373–4378.
[5] R. Yan, D.T. Liang, L. Tsen, Y.P. Wong, Y.K. Lee, Bench-scale experimental evaluation of carbon performance on mercury vapor adsorption, Fuel 83 (2004) 2401–2409.
[6] E. Malkoc, Y. Nuhoglu, Fixed bed studies for the sorption of chromium (VI) onto tea factory waste, Chem. Eng. Sci. 61 (2006) 4363–4372.
[7] S. Wang, H. Li, Kinetic modeling and mechanism of dye adsorption on unburned carbon, Dyes Pigments 72 (2007) 308–314.
[8] S.V. Krishnan, B.K. Gullett, W. Jozewicz, Sorption of elemental mercury by activated carbons, Environ. Sci. Technol. 28 (1994) 1506–1512.
[9] J. Luo, A.M. Hein, J.Y. Hwang, Adsorption of vapor phase mercury on various carbons, J. Miner. Mater. Charact. Eng. 3 (2004) 13–22.
[10] G.O. Wood, J.F. Stampfer, Adsorption rate coefficients for gases and vapors on activated carbons, Carbon 31 (1993) 195–200.
[11] S. Goswami, U.C. Ghosh, Studies on adsorption behavior of Cr(VI) onto synthetic hydrous stannic oxide, Water SA 31 (2005) 597–602.
[12] C.R. Reid, K. Thomas, Adsorption of gases on a carbon molecular sieve used for air separation: linear adsorptives as probes for kinetic selectivity, Langmuir 15 (1999) 3206–3218.
[13] M.H. Kalavathy, T. Karthikeyan, S. Rajgopal, L.R. Miranda, Kinetic and isotherm studies of Cu(II) adsorption onto H_3PO_4-activated rubber wood sawdust, J. Colloid Interface Sci. 292 (2005) 354–362.
[14] C.W. Cheung, J.F. Porter, G. McKay, Elovich equation and modified second order equation for sorption of cadmium ions onto bone char, J. Chem. Technol. Biotechnol. 75 (2000) 963–970.
[15] Z. Reddad, C. Gerente, Y. Andres, P. Le Cloirec, Adsorption of several metal ions onto a low cost biosorbent: kinetic and equilibrium studies, Environ. Sci. Technol. 36 (2002) 2067–2073.
[16] N.J. Foley, K.M. Thomas, P.L. Forshaw, D. Stanton, P.R. Norman, Kinetics of water vapour adsorption on activated carbon, Langmuir 13 (1997) 2083–2089.
[17] A.I. LaCava, V.A. Koss, D. Wickens, Non-Fickian adsorption rate behaviour of some carbon molecular sieves, Gas Sep. Purif. 3 (1989) 180–186.
[18] G. Skodras, Ir. Diamantopoulou, A. Zabaniotou, G. Stavropoulos, G.P. Sakellaropoulos, Enhanced mercury adsorption in activated carbons from biomass materials and waste tires, Fuel Process. Technol. 88 (2007) 749–758.
[19] E. Malcoc, Y. Nuhoglu, Fixed bed studies for the sorption of chromium (VI) onto tea factory waste, Chem. Eng. Sci. 61 (2006) 4363–4372.
[20] J.Y. Lee, Y. Ju, T.C. Keener, R.S. Varma, Development of cost-effective noncarbon sorbents for Hg^0 removal from coal-fired power plants, Environ. Sci. Technol. 40 (2006) 2714–2720.
[21] Hill G. Charles, Chemical Engineering Kinetics and Reactor Design, John Wiley & Sons Inc., New York, 1977, pp. 447–451.
[22] D.M. Ruthven, Principles of Adsorption and Adsorption Processes, John Wiley & Sons Inc., New York, 1984, pp. 213–214.
[23] Lee K.C. Vinci, Porter F. John, McKay Gordon, Fixed bed modeling for acid dye adsorption onto activated carbon, J. Chem. Technol. Biotechnol. 78 (2003) 1281–1289.

[24] S. Kwon, E. Borquet, R.D. Vidic, Impact of surface heterogeneity on mercury uptake by carbonaceous sorbents under UHV and atmospheric pressure, Environ. Sci. Technol. 36 (2002) 4162–4169.
[25] P. Englezos, N. Kalogerakis, Applied Parameter Estimation for Chemical Engineers, Marcel Deccer, Inc., 2001.
[26] G. Skodras, P. Grammelis, P. Basinas, S. Kaldis, E. Kakaras, G.P. Sakellaropoulos, A kinetic study on the devolatilisation of animal derived byproducts, Fuel Process. Technol. 88 (2007) 787–794.
[27] Y.S. Ho, G. McKAY, A comparison of chemisorption kinetic models applied to pollutant removal on various sorbents, Trans IchemE 76 (1998) 332–340.
[28] R.H. Perry, C.H. Chilton, Chemical ENGINEERS HANdbook, Fifth ed., International book company, 1974.
[29] D.H. Kim, Linear driving force formulas for diffusion and reaction in porous catalysts, AIChE J. 35 (1989) 343–346.
[30] S. Azizian, Kinetic models of sorption: a theoretical analysis, J. Colloid Interface Sci. 276 (2004) 47–52.
[31] H.K. Chagger, F.E. Ndaji, M.L. Sykes, K.M. Thomas, Kinetics of adsorption and diffusional characteristics of carbon molecular sieves, Carbon 33 (1995) 1405–1411.
[32] Y.S. Ho, G. McKay, The kinetics of sorption of divalent metal ions onto sphagnum moss peat, Wat. Res. 34 (2000) 735–742.
[33] M.A. Vannice, Kinetics of catalytic reactions. Springer Editions, 2005.
[34] Ho Yun-Shan, Review of second-order models for adsorption systems, J. Hazard. Mater. 136 (2006) 681–689.
[35] F. Banat, S.Al. Asheh, R.Al. Ahmad, F. Bni-Khalid, Bench-scale and packed bed sorption of methylene blue using treaded olive pomace and charcoal, Biores. Technol. 98 (2007) 3017–3025.
[36] D.J.M. Low, Kinetics of chemisorption of gases on solids, Chem. Rev. 60 (1960) 267–312.